Solid State Ionics 432 (2025) 117069

Contents lists available at ScienceDirect

Solid State Ionics

journal homepage: www.elsevier.com/locate/ssi

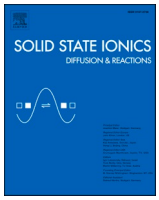

Polycarbonate-based polymer electrolytes for potassium batteries

Isabell Lee Johansson [a,b,1], Timofey I. Kolesnikov [b,c,1], Anna Khudyshkina [b], Ulf-Christian Rauska [b], Daniel Brandell [a], Jonas Mindemark [a], Guiomar Hernández [a], Fabian Jeschull [b,*]

[a] Department of Chemistry – Ångström Laboratory, Uppsala University, SE-751 21 Uppsala, Sweden
[b] Karlsruhe Institute of Technology (KIT), Institute for Applied Materials – Energy Storage Systems (IAM-ESS), Herrmann-von-Helmholtz-Platz 1, 76344 Eggenstein-Leopoldshafen, Germany
[c] Karlsruhe Institute of Technology (KIT), Institute for Chemical Technology and Polymer Chemistry (ITCP), Engesserstraße 18, 76131 Karlsruhe, Germany

ARTICLE INFO

Keywords:
Potassium battery
Solid polymer electrolyte
Poly(ε-caprolactone-*co*-trimethylene carbonate) (P(CL-TMC))
Poly(trimethylene carbonate) (PTMC)

ABSTRACT

Polycarbonate-based solid polymer electrolytes (SPEs) are being intensively studied for use in all-solid-state batteries as a viable alternative to the commonly used poly(ethylene oxide)-based SPEs. Specifically, poly(trimethylene carbonate) (PTMC) and poly(ε-caprolactone–*co*–trimethylene carbonate) (P(CL-TMC)) as a well-performing copolymeric derivative represent two materials classes that so far have not been studied in potassium battery applications. Herein, we aim to close this knowledge gap by studying physical material properties of PTMC and P(CL-TMC) solid electrolytes with potassium bis(trifluoromethanesulfonyl)imide (KTFSI) as conductive salt and examine their electrochemical stability and characteristics in K-metal/$K_2Fe[Fe(CN)_6]$ (KFF), as well as $Fe[Fe(CN)_6$/$K_2Fe[Fe(CN)_6]$ cell configurations. While operation of polycarbonate-based solid-state potassium batteries at temperatures as low as 40 °C is feasible, comparatively low discharge capacities and capacity retention were observed in comparison to polyether-based systems. For the P(CL-TMC) material, rapid degradation through depolymerization processes in direct contact with potassium metal represents a major bottleneck. With this study, we set a starting point for further materials development in alternative polymer hosts for SPE applications in potassium batteries.

1. Introduction

The growing demand for high-energy-density batteries has prompted significant interest in exploring alternative battery chemistries that are both environmentally friendly and based on more abundant raw material platforms than lithium-ion technology [1–5]. One such system is potassium batteries, which can achieve high energy density through comparatively high cell voltages, thereby offsetting the penalty of the larger atomic weight of potassium). In organic electrolytes, potassium metal exhibits the lowest standard redox potential in the series Li–Na–K [6,7], and positive electrode materials such as Prussian blue analogues (PBAs) or polyanionic compounds tend to achieve remarkably high redox potentials [8–10]. PBAs $K_2M[Fe(CN)_6]$ (M = Fe, Mn, *etc.*), are among the most promising materials for positive electrodes due to their high reversible capacity, long cycle life, and relatively high discharge voltage [11]. However, this poses challenges to the electrochemical stability of any electrolyte, particularly liquid electrolytes, highlighting the need for the development of novel electrolytes [12–14]. In addition, it has been demonstrated that the passivating surface layers formed in potassium systems are inherently less stable and more prone to dissolution and recurrent reformation [15–18]. This leads to low reversibility, increased cell resistance, rapid electrolyte consumption and consequently poor capacity retention, especially when K-metal is used [7,19–21]. In this regard, solid polymer electrolytes (SPEs) offer several advantages, particularly regarding their cathodic stability at the negative K-metal electrode and potentially battery safety [22,23]. Using SPEs based on poly(ethylene oxide) (PEO), the capacity retention of the K-metal/$K_2Fe[Fe(CN)_6]$ configuration could be greatly improved compared to a liquid electrolyte reference system [24,25]. In addition, the PEO-based K-ion conductors can operate at 55 °C, which is below the temperatures reported for corresponding Li- and Na-SPE systems [26–29]. Nonetheless, their generally low ionic conductivity, especially

* Corresponding author.
E-mail address: fabian.jeschull@kit.edu (F. Jeschull).
[1] These authors contributed equally to this work.

https://doi.org/10.1016/j.ssi.2025.117069
Received 8 September 2025; Received in revised form 24 October 2025; Accepted 3 November 2025
Available online 12 November 2025

at ambient (or near-ambient) temperatures, remains a limiting factor for PEO as a host material.

PEO is still the most widely studied SPE matrix, in contrast to conventional liquid electrolytes which are often based on carbonate solvents due to their role in the formation of a protective solid electrolyte interphase on the anodes used [30,31]. Ion conduction in carbonate-based polymer host materials, such as PTMC, is affected by higher glass transition temperatures (T_gs) and higher transference numbers owing to weaker coordination to Li^+ [32,33]. Both PTMC and P(CL-TMC) have mostly been studied with lithium- and sodium-based salts [34–37], but only to a lesser extent with other post-lithium systems [33,38,39].

To the best of our knowledge, there is only one study by Fei et al. [29] who successfully implemented a propylene carbonate-based SPE in a K-metal/perylenetetracarboxylic dianhydride configuration, showing notable improvements over a corresponding liquid electrolyte system. Neither PTMC nor P(CL-TMC) have been studied so far for their application as host material in SPEs for potassium batteries. To close this gap, we focus herein on the physical and electrochemical characteristics of PTMC and P(CL-TMC) solid electrolytes with potassium bis(trifluoromethylsulfonyl)imide (KTFSI) as conductive salt in a range of different polymer-to-salt compositions. The best-performing PTMC:KTFSI and P(CL-TMC):KTFSI electrolytes were further studied in electrochemical tests in K/K symmetrical cells, $K/K_2Fe[Fe(CN)_6]$ cells and $Fe[Fe(CN)_6]/K_2Fe[Fe(CN)_6]$ configurations to explore their anodic and cathodic stability against different electrode materials.

2. Experimental

2.1. Materials

Trimethylene carbonate (TMC, Obiter Research), ε-caprolactone (CL, 99 % Sigma Aldrich, distilled under reduced pressure over CaH_2), Sn(Oct)$_2$ (95 %, Sigma-Aldrich) prepared as a 1 M solution in toluene (extra dry, over molecular sieves, 99.8 %, AcroSeal®, Acros Organics), potassium bis(trifluoromethanesulfonyl)imide (KTFSI, 99.5 wt%, Solvionic, dried at 110 °C for 12 h under vacuum), ethylene carbonate (EC, anhydrous, 99 % Sigma Aldrich), propylene carbonate (PC, anhydrous, 99 % Sigma-Aldrich), fluoroethylene carbonate (FEC 99 % Sigma-Aldrich) and acetonitrile (anhydrous, 99.8 %, Sigma-Aldrich). All samples were stored, handled, and prepared in an argon-filled glove box.

2.2. Polymer and copolymer synthesis

Poly(trimethylene carbonate) (M_w = 274,400 g mol^{-1}, M_n = 131,900 g mol^{-1}) and poly(ε-caprolactone-*co*-trimethylene carbonate) with 80:20 molar ratio CL:TMC (M_w = 703,600 g mol^{-1}, M_n = 312,100 g mol^{-1}), were both synthesized through ring-opening polymerization of the respective monomers and a Sn(Oct)$_2$ catalyst, following previously reported synthetic procedures [34,40]. In brief, the polymerization of 0.2 mol of TMC or TMC:CL monomer mixtures, with 40 μL of a 1 M Sn(Oct)$_2$ catalyst solution in toluene a stainless steel reactor was heated to 130 °C for 3 days. The reactor was cooled down and transferred to a glovebox, where the polymer was removed.

2.3. Polymer characterization

^{1}H NMR spectra were recorded using a Bruker Ascend 400 NMR spectrometer (Germany) with a working frequency of 400 MHz using acetonitrile-d_3 (Merck ≥99.8 atom % D) as solvent. Gel permeation chromatography (GPC) measurements were performed on an Agilent 1260 Infinity (Agilent Technologies) GPC system, in anhydrous tetrahydrofuran, 1 mL min^{-1}, at 35 °C. Poly(methyl methacrylate) standards were used to calibrate the system. Attenuated total reflectance-Fourier transform infrared (ATR-FTIR) spectra were recorded in the range of 4000–500 cm^{-1} on a Platinum ATR spectrometer (Bruker).

2.4. Solid polymer electrolyte preparation

KTFSI and PTMC or PCL-PTMC were dissolved in acetonitrile and stirred overnight, the polymer solutions were then poured into Teflon molds and the solvent was removed by keeping them in an oven at 30 °C for 20 h at a reduced pressure of 200 mbar, followed by heating at 60 °C for 40 h and vacuum (10^{-3} bar). The dry polymer electrolyte films were then cut to the required size and the thickness was measured with thickness gauge.

The salt concentration in the polymer electrolytes varied and the samples are distinguished by molar ratio of polymer carbonate (and ester) units to K^+ ions: PTMC$_n$KTFSI, n = 24, 20, 16, 12, 8, 4, 2, and 1. P(CL$_m$TMC$_n$)KTFSI, $(m + n)$ = 24, 20, 16, 12, 8, 4, 2, and 1.

2.5. Liquid electrolyte preparation

Liquid electrolyte was used as a reference system for comparison with the solid polymer electrolyte cells. For this, a solution of 0.5 M KPF_6 in ethylene carbonate and propylene carbonate (EC:PC, 1:1 *V*/V ratio) and 2 wt% FEC was prepared. During cell assembly 150 μL of the solution was filtered and used with a glass fiber separator (cut to 19 mm diameter, previously dried for 12 h at 120 °C).

2.6. Differential scanning calorimetry

A Mettler Toledo DSC 3+ system was used for differential scanning calorimetry (DSC) measurements. Between 5 and 10 mg of sample was weighed and hermetically sealed in aluminum pans. The samples were heated from room temperature to 200 °C at a heating rate of 10 K min^{-1}, and cooled to −70 °C at a cooling rate of −10 K min^{-1}. Two heating–cooling cycles were performed on the samples to remove any thermal history, and the glass transition temperature was determined from the midpoint of the glass transition step during the second heating scan.

2.7. Ionic conductivity

The polymer electrolyte films were cut to a diameter of 12 mm and then sandwiched between two stainless steel electrodes in CR2025-type coin cells. A Teflon spacer, with inner diameter of 13 mm and a thickness of 50 μm, was used to center the polymer electrolyte film and to prevent it from changing dimensions during heating. The cells were pre-treated by annealing at 100 °C for 1 h a day prior to the measurements to improve interfacial contact with the electrodes and the electrolyte film. The ionic conductivity was then determined by electrochemical impedance spectroscopy (EIS) measurements on a Schlumberger SI 1260 Impedance/Gain-Phase Analyzer over a frequency range of 1 Hz to 10 MHz and a voltage amplitude of 10 mV. Measurements were taken in the temperature range from 25 to 85 °C. The bulk resistance of the electrolyte was then determined by fitting with a Debye circuit to the data in the Nyquist plot.

2.8. Composite electrode preparation

Composite electrodes were prepared using $K_2Fe[Fe(CN)_6]$ (KFF) or $Fe[Fe(CN)_6]$ (FF) as active materials [41,42]. The electrode slurries were prepared by mixing 0.180 g (44.8 wt%) of active material KFF or FF, 0.090 g (22.4 wt%) of carbon black (Timcal super C65), 0.030 g (7.5 wt %) PVdF (Solef PVDF 1013/1001 R6090), 0.030 g (7.5 wt%) of P(CL-TMC), and 0.0714 g (17.8 wt%) of KTFSI in 3 mL of *N*-methyl-2-pyrrolidone (99.5 wt%, Sigma-Aldrich). The KFF electrodes were cut to a diameter of 12 mm and dried at 110 °C for 12 h under vacuum, and the FF electrodes were cut to a diameter of 16 mm and dried at 80 °C for 12 h under vacuum.

2.9. Cell assembly

AAll cells were prepared either as coin cells or as pouch cells, with Cu and Al tabs. In the pouch cells, a PE-film, with a circular hole cut to the same diameter as the working electrode (KFF), was placed between the aluminum tab and the SPE, this was done to avoid any potential corrosion reaction between the TFSI and aluminum. The anodes were either metallic potassium or FF electrodes. The SPE composition was either P(CL-TMC):KTFSI (12,1) or PTMC:KTFSI (16,1).

2.10. SPE stability with potassium metal

Plating-stripping experiments were performed in symmetrical coin cells using potassium metal electrodes with a diameter of 14 mm and an SPE with a diameter of 16 mm. During each cycle, the cell was charged/discharged for 2 h at 7.5 μA cm^{-2} at 40 °C. Cells cycled with potassium metal and P(CL-TMC) were disassembled inside the glovebox and a viscous polymer residue was collected from the back side of the coin cell spacer and dissolved in acetonitrile-d_3 for NMR analysis. Polymer electrolyte was also collected from cells cycled with potassium metal, and polymers stored in contact with potassium metal, for GPC measurements.

2.11. Cycling experiments

Galvanostatic cycling was performed at a rate of C/20 (1C = 141 mAh g^{-1}, for $K_{1.9}Fe[Fe(CN)_6]$ [24,25]) at 40 °C with KFF as working electrode, and either metallic potassium or FF as the counter electrode within the voltage limits of 2.5–4.3 V *vs.* K^+/K and − 1.8–1.8 V *vs.* K^+/K, respectively.

Cut-off increase cell cycling (CICC) was performed to study the electrochemical stability and the resistance of the electrolytes. Following the previously described procedure [43], KFF was used as working electrode and metallic potassium as the counter electrode with the SPE sandwiched between them. The cells were cycled at a rate of C/20 at 40 °C, using a lower cut-off voltage of 3.0 V. The upper cut-off voltage was increased step-wise by 0.1 V every five cycles, starting from an initial value of 3.7 V *vs.* K^+/K, until the upper limit of 5.0 V *vs.* K^+/K.

3. Results & discussion

3.1. Synthesis and electrolyte properties

Stannous octotate ($Sn(Oct)_2$) is a widely used catalyst for initiating ring-opening polymerization of trimethylene carbonate, ε-caprolactone [44,45] and similar cyclic carbonate and carboxylate ester monomers. The polymers were synthesized using previously published procedures [40,46] and the synthetic route is shown in Scheme 1. For the synthesis of random P(CL-TMC) copolymer, a 80:20 monomer molar ratio between ε-caprolactone and trimethylene carbonate was targeted as it has previously shown the best tradeoff between ionic conductivity, amorphicity and cation transference number. Chemical structures were confirmed using NMR and FTIR spectroscopy. The assigned ^{1}H NMR spectra (**Fig. S1–2**) and FTIR spectra (**Fig. S3–4**) are in good agreement with previously published data [47,48]. Both polymers exhibit high molecular weight with an average molar mass (M_n) of around 131,900 g mol^{-1} and 312,100 g mol^{-1} for PTMC and P(CL-TMC), respectively. High M_n is required to prepare self-standing solid polymer electrolyte films with sufficient mechanical properties. DSC thermograms of pristine polymers are shown in **Fig. S5**. PTMC exhibits a glass transition temperature of −15 °C and shows no endothermic effects, confirming its amorphous structure, consistent with literature for high-molecular-weight PTMC [49]. In contrast, the P(CL-TMC) copolymer has a lower glass transition temperature of −57 °C. Additionally, due to the high fraction of semi-crystalline caprolactone repeating units, P(CL-TMC) displays an exothermic effect with a crystallization peak at −24 °C and an endothermic melting peak at 15 °C. A lower glass transition temperature generally corresponds to increased mobility of the polymer backbone, which should promote ion transport. Thermal properties of the pristine polymers are summarized in **Table S1**.

Differential scanning calorimetry measurements were performed on PTMC:KTFSI and P(CL-TMC):KTFSI compositions at different ratios, see Fig. 1 and **Table S2**, to evaluate the thermal properties of these electrolytes. The glass transition temperature (T_g) for the different compositions is shown in Fig. 1a and b, as an indicator of polymer chain mobility. While increasing the amount of the amorphous phase is an often desired outcome for PEO-based electrolytes, the thermograms of the PTMC system indicate full amorphicity (Fig. 1a) and the P(CL-TMC) blends are amorphous when the salt concentration exceeds a C=O:K^+ ratio of 16:1 (except for 12:1 P(CL-TMC) blend), which shows a melting peak at 25 °C) (Fig. 1b). A similar trend has been previously reported for PEO:KTFSI compositions, where SPEs with a 12:1 molar ratio predominantly exhibit amorphous behavior, whereas those with other ratios remain semi-crystalline [24]. Compositions of P(CL-TMC):KTFSI with 24:1 and 20:1 molar ratios showed exothermic effects corresponding to crystallization and endothermic effects of melting, indicating that this low amount of salt is not able to disrupt the crystallinity of the polymer. Generally, in both SPE systems, the T_g shifts to higher values with increasing salt concentration, which is ascribed to restrictions in the degrees of freedom of polymer chains or segments [50], for instance due to interchain coordinate bonds between potassium ions and polymer chains [51].

PTMC:KTFSI samples maintained T_gs around −15 °C at concentrations below 8:1 and showed a more rapid increase at concentrations above 8:1, whereas the P(CL-TMC):KTFSI blends demonstrate a more linear increase of T_g over the examined range of salt concentrations. At high salt concentrations (1:1 and 2:1), endothermic processes appear at temperatures between 100 and 170 °C (lower than the melting temperature of KTFSI salt at 200 °C) that are likely associated with melting of undissolved KTFSI salt in the polymer matrix. The P(CL-TMC):KTFSI electrolytes also have a much lower T_g compared to the PTMC electrolytes. This is also the case with LiTFSI electrolytes of these polymers, since the introduction of PCL to the polymer chain lowers the T_g [52].

The main difference in the glass transition behavior of the SPEs is that PTMC is amorphous, whereas P(CL-TMC) is semi-crystalline. At DSC

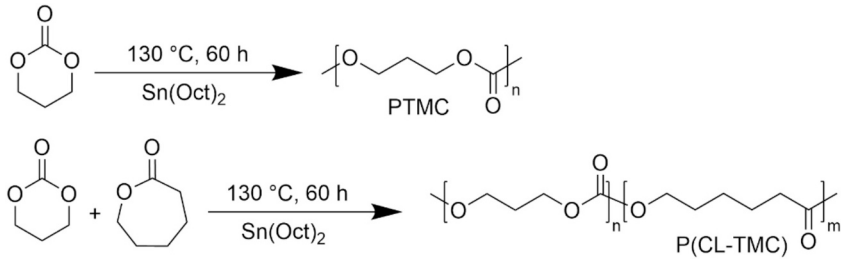

Scheme 1. Synthetic scheme of PTMC and P(CL-TMC).

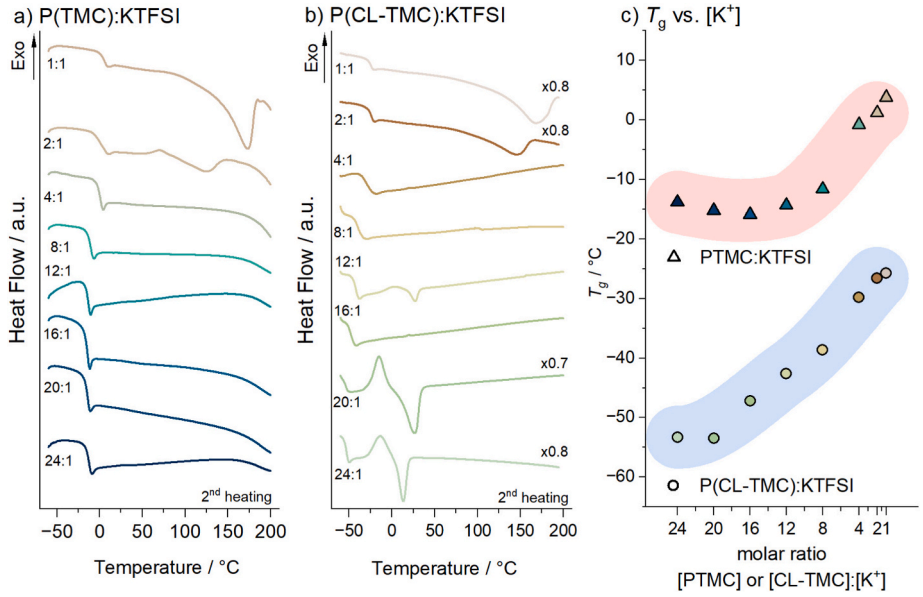

Fig. 1. DSC thermograms of the second heating scan of (a) PTMC:KTFSI and (b) P(CL-TMC):KTFSI with different molar ratios of PTMC:K^+ or P(CL-TMC):K^+. (c) Dependency of T_g on the PTMC:K^+ or P(CL-TMC):K^+ molar ratio. The broad lines only indicate the polymer electrolyte host materials as either (red) PTMC or (blue) P(CL-TMC).

curves of PTMC there is no endothermic effect up to 8:1 ratio and T_g remains unchanged at approximately −15 °C. While PTMC is able to dissolve the KTFSI salt and no endothermic melting peak of crystalline regions is observed, T_g remains unchanged at approximately −15 °C, up to 8:1 ratio. Once the saturation limit is reached and undissociated KTFSI is present in the SPE, T_g begins to increase. In contrast, for P(CL-TMC), a semi-crystalline phase is always present, and T_g consistently increases with salt content. A similar trend was observed for P(CL-TMC)-based SPEs with LiTFSI, where glass transition increases at an approximate ratio 1:5 [40].

The total bulk ionic conductivity was measured for both PTMC:KTFSI and P(CL-TMC):KTFSI systems over a temperature range from 25 °C to 85 °C. The conductivity for a specific temperature as a function of concentration is presented in Fig. 2 and the Arrhenius plots are presented in **Fig. S6**. The ionic conductivity is generally higher for P(CL-TMC):KTFSI electrolytes than for PTMC:KTFSI electrolytes, with the highest ionic conductivities found for P(CL-TMC):KTFSI (12:1), *e.g.* 0.34 mS cm^{-1} at 85 °C. At 55 °C, the ionic conductivities dropped to the range of 10^{-5} to 10^{-6} S cm^{-1} for all polymer-to-salt ratios investigated. In comparison with previously published PEO:KTFSI 16:1 system [24] the ionic conductivities at room temperature were about one order of magnitude lower for the P(CL-TMC):KTFSI compositions (highest value 6•10^{-6} S cm^{-1}), and three orders of magnitude for PTMC:KTFSI electrolytes. In the comparison in Fig. 2, the highest ionic conductivities for the PTMC:KTFSI blends were generally one order of magnitude lower than for compositions of P(CL-TMC):KTFSI, which is a result of the higher chain mobility (based on the thermal properties in Fig. 1) of the P(CL-TMC) copolymer. At low salt contents, the limited concentration of

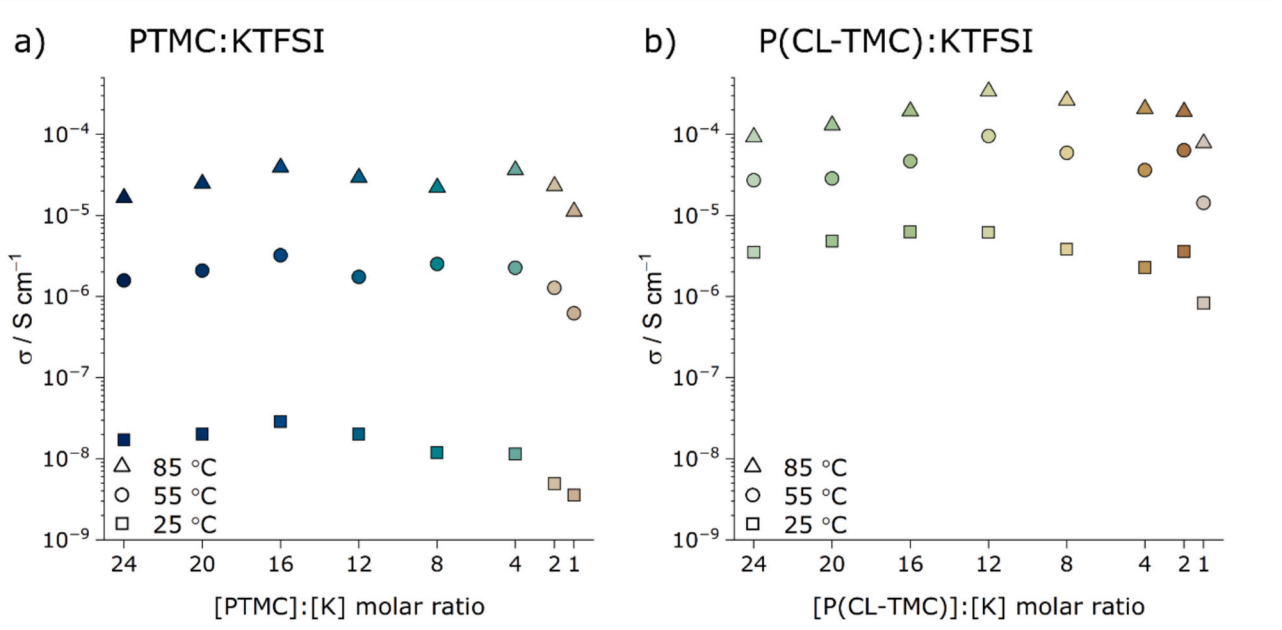

Fig. 2. Ionic conductivity isotherms of PTMC:KTFSI (a) and P(CL-TMC):KTFSI (b) compositions for selected temperatures at 25 °C, 55 °C and 85 °C.

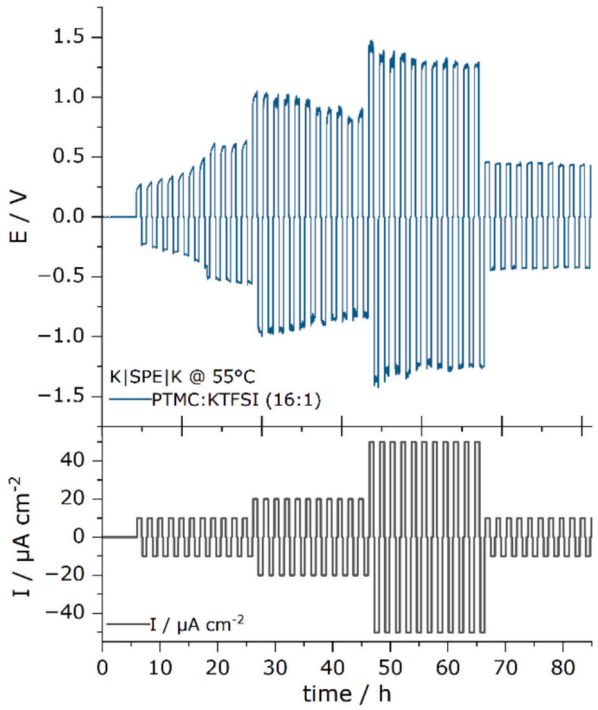

Fig. 3. Stripping-plating experiments performed at 55 °C in a symmetrical cell with PTMC:KTFSI (16:1) electrolyte sandwiched between two potassium electrodes (10 mm in diameter) at current densities of 10, 20 and 50 µA cm^{-2}.

charge carriers and a residual degree of crystallinity in the semi-crystalline P(CL-TMC) electrolytes impede the ion transport. The ionic conductivity then increases with concentration, having a maximum at 12:1 polymer-to-salt ratio. Beyond the 8:1 composition, a notable drop in conductivity is seen due to the formation of ion pairs and aggregates. In contrast, the amorphous PTMC electrolytes feature smaller changes in ionic conductivity (although a slight maximum is observed at 16:1) in agreement with the small changes observed in T_g. However, above PTMC:K ratios of 4:1, the ionic conductivity decreased as the T_g starts to increase. For PCL the coordination strength was found to be generally lower than for PEO (strongly chelating) and to decrease in the order $Li^+ > Na^+ > K^+$ [53], which can give rise to ion pairing and ion clustering effects. Comparing polyesters and polycarbonates, experiments with LiTFSI suggest stronger ion–dipole interaction between Li^+ and PCL compared to PTMC [33]. Corresponding DFT calculations have also shown that Li^+ coordinates stronger to the (CL) ester groups than the carbonate groups of TMC [52]. P(CL-PTMC) copolymers maintain a higher chain flexibility than the PTMC mixtures, which will also promote higher ionic conductivities. Since the compositions with highest ionic conductivity were P(CL-TMC):KTFSI (12:1) and PTMC:KTFSI (16:1), these were selected for the subsequent cell tests.

3.2. Stability against potassium metal

The PTMC:KTFSI and P(CL-TMC):KTFSI electrolytes were first studied in K|SPE|K symmetrical cells for their stripping-plating behavior in the range from 10 to 50 µA cm^{-2}. The voltage transient in Fig. 3 of the PTMC:KTFSI (16:1) electrolyte at 55 °C displays gradually increasing overpotentials in the range from 250 to 640 mV already at the smallest current density of 10 µA cm^{-2}. Already at current densities of 20 µA cm^{-2} the stripping/plating potential reached more than 1.0 V. Interestingly, after returning to lower current densities, the reaction potential stabilized at voltages of around ±450 mV. A second cell that was tested under slightly altered conditions at 40 °C failed after only a few cycles (**Fig. S7a**). A PEO-based block copolymer tested under the same conditions in a previous study showed plating/stripping voltages of around 100 mV at 10 µA cm^{-2} that remained constant over the three different current sequences [22,28]. Considering that the ionic conductivity is an order of magnitude lower for P(CL-TMC), than for PEO-based SPEs, higher stripping/plating potentials are to be expected. This experiment also highlights a major problem in potassium cell chemistries, related to the reactivity of the alkali metal towards any electrolyte and the formation of resistive electrode-electrolyte interphases.

In contrast, with the P(CL-TMC):KTFSI SPE, all experiments lead to cell failure, presumably due to degradation of polymer in contact with potassium metal (**Fig. S7b**). The cells contained a viscous liquid residue underneath the coin cell spacer after the test. Moreover, the solid and self-standing P(CL-TMC):KTFSI electrolyte film changed shape visibly.

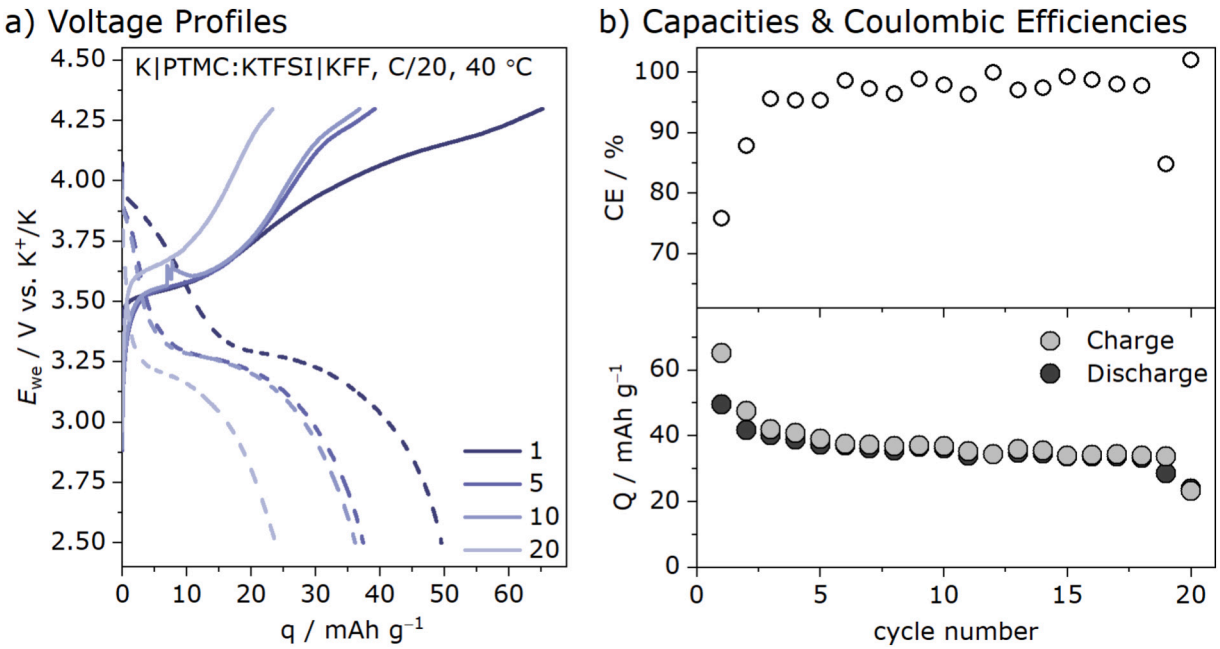

Fig. 4. Galvanostatic cycling (C/20 at 40 °C) of K|PTMC:KTFSI|KFF half-cell showing, (a) the voltage profiles (2.5–4.3 V *vs.* K^+/K) of selected cycles (#1, #5, #10, #20), (b) corresponding coulombic efficiency, and capacity retention over the first 20 cycles.

In a follow-up experiment, the liquid residue was extracted and analyzed by ^{1}H NMR spectroscopy (**Fig. S8**) and GPC (**Table S3**). In the spectrum the signal at 3.46 ppm can be attributed to CH_2–OH end groups that allow an estimation of the degree of polymerization (DP) of P(CL-TMC). A significant decrease in the relative signal intensities between the P(CL-TMC) backbone and the CH_2–OH end groups at 3.46 ppm suggests that the DP of P(CL-TMC) dropped from 174 to 18 [54]. This hypothesis was further strengthened by the decrease in molecular weight seen by GPC. In contrast to the copolymer, the PTMC:KTFSI cells did neither displayed any visible degradation of the polymer electrolyte, nor did GPC show any notable change in molecular weight under the experimental conditions (**Table S3**), indicating good stability towards potassium metal. Previous work by Wildersinn et al. [55] shows that the potassium metal surface mainly consists of K_2CO_3 and KOH, even when handled in a glovebox atmosphere with sub-ppm H_2O and O_2 concentrations. The depolymerization process could be initiated by these surface groups, rendering P(CL-TMC) more prone to this process in presence of hydroxyl groups than PTMC [56].

3.3. Cycling experiments

Galvanostatic cycling experiments were performed with both the PTMC:KTFSI and P(CL-TMC):KTFSI SPEs in half-cells against a KFF positive electrode (C_{th} = 155 mAh g^{-1}) at 40 °C and at a constant current of C/20 (Fig. 4). The P(CL-TMC):KTFSI cell showed high cell polarization and rapid capacity decay (**Fig. S9**), which are attributed to polymer degradation and will therefore not be further discussed in this section. The PTMC:KTFSI cell showed, unexpectedly, higher capacities and overall more consistent electrochemical behavior at 40 °C than at 55 °C. For the discussion herein, we therefore focus on the results at 40 °C (results at 55 °C are shown in **Fig. S10**). The cell in Fig. 4 showed an initial specific discharge capacity of 50 mAh g^{-1} and a notable capacity decrease by 24 % (38 mAh g^{-1}) over the following 5 cycles after which capacity loss slowed down until the 19th cycle (Fig. 4a). By the 20th cycle, the discharge capacity decreased to less than half the discharge capacity of the 1st cycle. The voltage profiles (Fig. 4b) show no gradual potential shifts due to additional polarization, except for the upper voltage plateau upon the oxidation of KFF that did not fully develop within the set voltage window and disappeared almost entirely on the

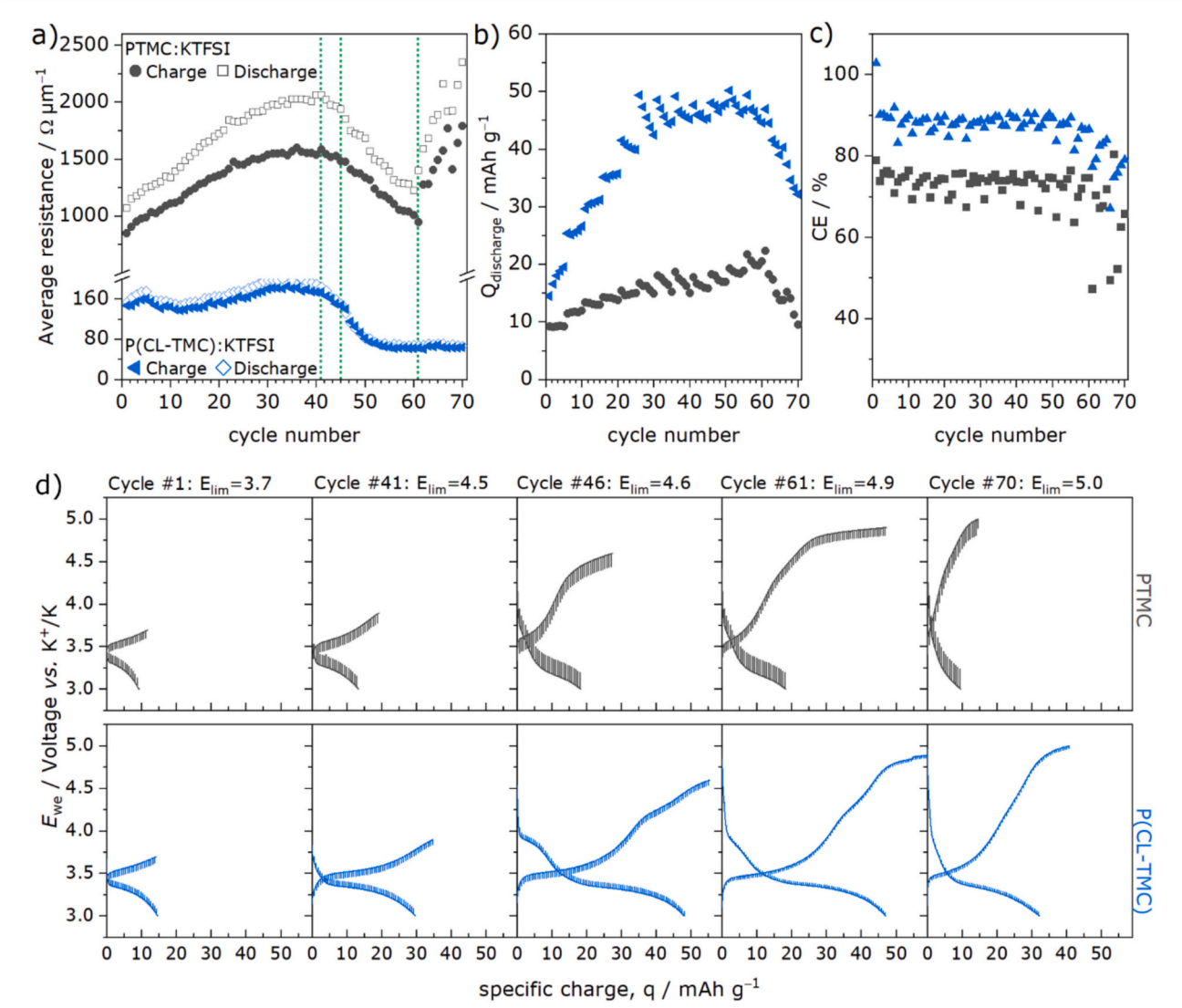

Fig. 5. Galvanostatic cycling with increasing the upper cut-off potential every fifth cycle of (black) K|PTMC:KTFSI (16:1)|KFF and (blue) K|P(CL-TMC):KTFSI (12:1)|KFF performed at 40 °C. a) Average resistance normalized by the thickness of each polymer electrolyte film, during charging and discharging. The green dotted lines show the transition to an upper cut-off of 4.5 (cycle 41), 4.6 (cycle 46), and 4.9 V (cycle 61) *vs.* K^+/K. b) Coulombic efficiency and c) specific discharge capacity during cycling. d) Voltage profiles of K|PTMC:KTFSI|KFF and K|P(CL-TMC):KTFSI|KFF at cycles 1, 41, 46, 61, and 70.

following cycles. Compared to the room temperature liquid electrolyte cell, which shows a characteristic plateau at 3.5 V *vs.* K^+/K, the lower voltage plateau of the PTMC cell is shifted by 120 mV (3.62 V *vs.* K^+/K). A decisive factor in regard to the comparatively poor specific capacities is the near-ambient operating conditions at 40 °C that led to a low ionic conductivity and thus a large internal cell resistance. P(CL-TMC) electrolytes had poor mechanical properties already at room temperature, as also observed previously [57]. A lower operation temperature of 40 °C was chosen to avoid that the electrolyte film loses its mechanical integrity entirely at elevated temperatures, as it shows liquid-like behavior already at room temperature. Hence, for consistency, PTMC-based electrolytes were also tested at 40 °C.

Cut-off increase cell cycling (CICC). Galvanostatic cycling with increasing upper cut-off potential (CICC) [43] was performed on K|SPE|KFF cells to investigate the electrochemical stability of SPEs at 40 °C. The specific discharge capacities, and corresponding resistances and coulombic efficiencies are shown for both electrolytes in Fig. 5a-c. In Fig. 5d selected voltage profiles are presented for further details. Although P(CL-TMC) did degrade in all other cell setups, it seemed to have withstood the CICC cycling experiment. There are several potential reasons for this behavior related to differences in the cycling protocol. For instance, a lower current was applied with a considerably longer step time than in the stripping-plating experiment. Furthermore, the intermittent relaxation sequences reduce the build-up of pronounced concentration gradients and cation depletion at the interface. Overall, this may have supported the formation of a protective surface layer and reduced dendritic growth as well as concentration overpotentials.

The P(CL-TMC):KTFSI (12:1) electrolyte has a higher ionic conductivity than the PTMC:KTFSI (16:1) electrolyte, which is reflected in the lower resistance and higher specific capacity in the P(CL-TMC) cell. In the PTMC-based cells the cut-off voltages are reached prematurely due to high overpotentials (Fig. 5b).

The resistance and specific capacity for both cells increase up until cycle 41 (upper cut-off 4.5 V *vs.* K^+/K), for five cycles the specific capacity remains fairly constant while the resistance of the cells decreased slightly. Once the was pushed beyond the limit of 4.5 V (*i.e.* upper cut-off 4.6–4.9 V *vs.* K^+/K; between cycle 46–61), the cell resistances in both cells decreased unexpectedly. For PTMC–based cells the charge capacity gradually increases above 4.6 V *vs.* K^+/K, while the discharge capacity remain low in a narrow window of 10–20 mAh g^{-1}, indicating that the degree of parasitic reactions increased considerably. This could be associated with a lower resistance, if at this point the electrode reaction is only a minor contributor. Reaching the upper limit of 5.0 V *vs.* K^+/K at cycle 61, the PTMC cell showed a steep increase in resistance, indicating accelerated cell failure. In contrast, the resistance of the P(CL-TMC) cell starts to decay around the cut-off limit of 4.5–4.6 V *vs.* K^+/K. Similar to the PTMC-electrolyte, there is a notable increase in the charge capacity above this voltage threshold due to high levels of irreversible reactions that accelerate the cell's decay. Accordingly, the coulombic efficiencies showed gradually decreasing values, above 4.5 V *vs.* K^+/K (Fig. 5c).

Although CICC experiments demonstrated that both polymers exhibit limited electrochemical stability high voltage cut-offs, both electrolytes display better properties than most liquid electrolytes, particularly at elevated temperatures. Beyond 4.5–4.6 V *vs.* K^+/K the degrees of parasitic reactions increase considerably, which is also well beyond the redox potential (and upper potential cut-off) of the KFF cathode. The low specific capacities in K-based cells are partly a result of their comparatively low ionic conductivity at 40 °C.

Asymmetric Cell Test with Prussian White & Berlin Green. In order to avoid the depolymerization of P(CL-TMC) and other instabilities with K metal, the anode material was exchanged from metallic potassium to iron hexacyanoferrate ($Fe[Fe(CN)_6]$, FF), *i.e.* Berlin green. The voltage of these cells, seen in Fig. 6, is expectedly lower compared to the cells with metallic anode. The specific capacity is low (around 35 mAh g^{-1}) compared to the theoretical capacity of the KFF material, which is partially due to the high resistance and overpotential. However, the P(CL-TMC) cell cycled for over 50 cycles with a C.E. of 95 %. Therefore, cycling of the P(CL-TMC) SPE was feasible in potassium cells without the use of potassium metal or prolonged pre-cycling at low cut-offs (as with CICC experiments).

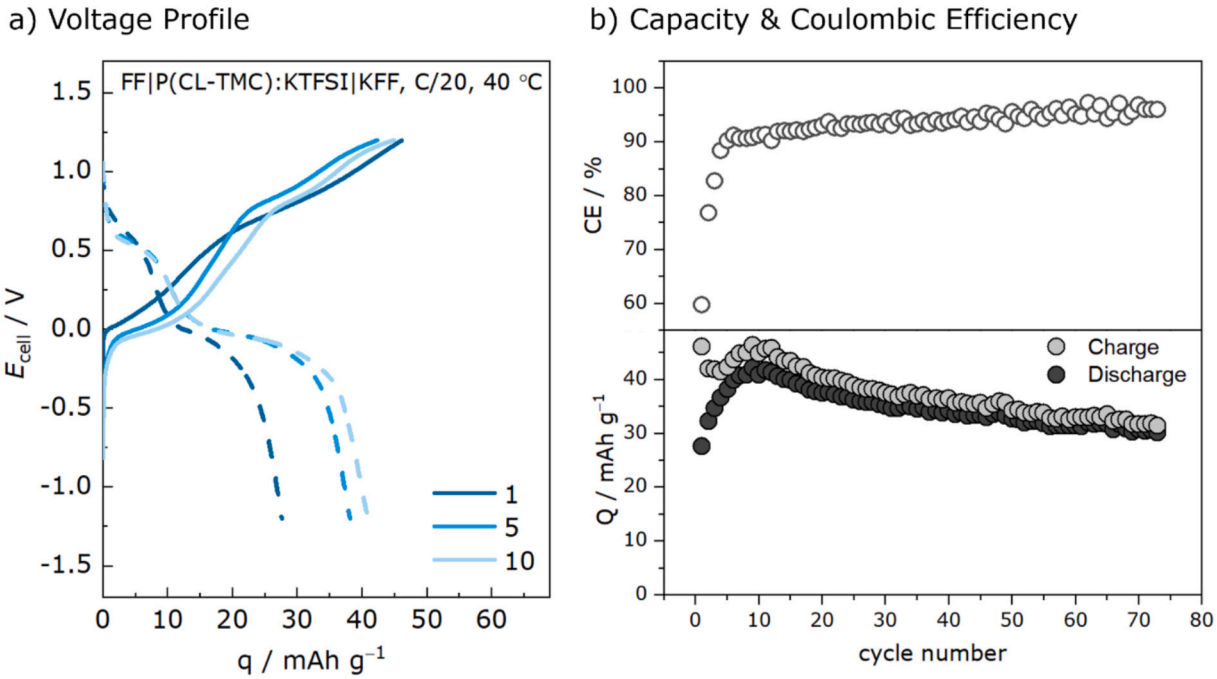

Fig. 6. (a) The voltage profile, and (b) coulombic efficiency, and specific capacity during galvanostatic cycling of a semi-symmetric cell with P(CL-TMC):KTFSI (12:1) electrolyte (−1.2–1.2 V *vs.* K^+/K, 40 °C) cycled at C/20.

4. Conclusions

In summary, we investigated the feasibility of utilizing polyesters and polycarbonates in all-solid-state potassium-based batteries. The SPEs based on P(CL-TMC) have both higher ionic conductivities and lower glass transition temperatures than the PTMC SPEs. Both properties are important for a well-functioning polymer electrolyte; however, a lack of compatibility between P(CL-TMC) and metallic potassium (due to depolymerization) severely limits the possibility of using this SPE in cells with metallic potassium. In a whole-cell setup, using iron hexacyanoferrate as anode instead, P(CL-TMC):KTFSI could be cycled. While the PTMC:KTFSI electrolyte can be cycled with a metallic potassium anode, the high resistance in these cells limits the specific capacity during galvanostatic cycling at 40 °C. Further work, not only focusing on the electrolyte but also on the anode and the cathode materials, should be done in order to improve the interfacial compatibility and practical capacity of these polycarbonate-based cells.

CRediT authorship contribution statement

Isabell Lee Johansson: Writing – review & editing, Writing – original draft, Methodology, Investigation, Formal analysis, Data curation. **Timofey I. Kolesnikov:** Writing – review & editing, Writing – original draft, Investigation, Formal analysis, Data curation. **Anna Khudyshkina:** Writing – review & editing, Methodology, Investigation, Formal analysis, Data curation, Conceptualization. **Ulf-Christian Rauska:** Writing – review & editing, Investigation, Formal analysis, Data curation. **Daniel Brandell:** Writing – review & editing, Supervision, Resources, Funding acquisition. **Jonas Mindemark:** Writing – review & editing, Writing – original draft, Supervision, Project administration, Conceptualization. **Guiomar Hernández:** Writing – review & editing, Writing – original draft, Supervision, Project administration, Funding acquisition, Conceptualization. **Fabian Jeschull:** Writing – review & editing, Writing – original draft, Supervision, Project administration, Funding acquisition, Conceptualization.

Declaration of competing interest

The authors declare the following financial interests/personal relationships which may be considered as potential competing interests: Guiomar Hernandez reports financial support was provided by German Research Foundation. Fabian Jeschull reports financial support was provided by German Research Foundation. Daniel Brandell reports financial support was provided by European Research Council. If there are other authors, they declare that they have no known competing financial interests or personal relationships that could have appeared to influence the work reported in this paper.

Acknowledgements

This work contributes to the research performed within the Post Lithium Storage Cluster of Excellence (POLiS). G.H. thanks the POLiS Cluster for the Award of Excellence for Female Researchers given in 2022. The European Research Council (grant no. 771777 FUN POLYSTORE) is acknowledged for their financial support and STandUP for Energy and COMPEL for their base funding. This work contributes to the research performed at CELEST (Center for Electrochemical Energy Storage Ulm-Karlsruhe) and was funded by the German Research Foundation (DFG) under Project ID 390874152 (POLiS Cluster of Excellence, EXC 2154). The authors thank Celine Röder and Iurii Panasenko for the synthesis of (potassium) iron hexacyanoferrate and preparation of composite electrode coatings, as well as Jan-Felix Schuster for his support with the liquid electrolyte cell tests. Darius B Shemirani is acknowledged for conducting the GPC measurements.

Appendix A. Supplementary data

Supplementary data to this article can be found online at https://doi.org/10.1016/j.ssi.2025.117069.

Data availability

Data will be made available on request.

References

[1] K. Kubota, M. Dahbi, T. Hosaka, S. Kumakura, S. Komaba, Towards K-ion and Na-ion batteries as “beyond Li-ion.”, Chem. Rec. 18 (4) (2018) 459–479, https://doi.org/10.1002/tcr.201700057.
[2] H. Wang, D. Yu, C. Kuang, L. Cheng, W. Li, X. Feng, Z. Zhang, X. Zhang, Y. Zhang, Alkali metal anodes for rechargeable batteries, Chem 5 (2) (2019) 313–338, https://doi.org/10.1016/j.chempr.2018.11.005.
[3] A. V, B. John, M. Td, Potassium-ion batteries: key to future large-scale energy storage? ACS Appl Energy Mater 3 (10) (2020) 9478–9492, https://doi.org/10.1021/acsaem.0c01574.
[4] F. Duffner, N. Kronemeyer, J. Tübke, J. Leker, M. Winter, R. Schmuch, Post-Lithium-ion battery cell production and its compatibility with Lithium-ion cell production infrastructure, Nat. Energy 6 (2) (2021) 123–134, https://doi.org/10.1038/s41560-020-00748-8.
[5] A. Mauger, C.M. Julien, A. Paolella, M. Armand, K. Zaghib, A comprehensive review of Lithium salts and beyond for rechargeable batteries: progress and perspectives, Mater. Sci. Eng. R. Rep. 134 (2018) 1–21, https://doi.org/10.1016/j.mser.2018.07.001.
[6] S. Komaba, T. Hasegawa, M. Dahbi, K. Kubota, Potassium intercalation into graphite to realize high-voltage/high-power potassium-ion batteries and potassium-ion capacitors, Electrochem. Commun. 60 (2015) 172–175, https://doi.org/10.1016/j.elecom.2015.09.002.
[7] I. Panasenko, M. Bäuerle, F. Jeschull, How reference electrodes improve our understanding of degradation processes in half and full cell potassium-ion battery setups, Electrochim. Acta 513 (2025) 145551, https://doi.org/10.1016/j.electacta.2024.145551.
[8] H. Kim, D.-H. Seo, M. Bianchini, R.J. Clément, H. Kim, J.C. Kim, Y. Tian, T. Shi, W.-S. Yoon, G. Ceder, A new strategy for high-voltage cathodes for K-ion batteries: stoichiometric KVPO4F, Adv. Energy Mater. 8 (26) (2018) 1801591, https://doi.org/10.1002/aenm.201801591.
[9] C. Vaalma, D. Buchholz, S. Passerini, Non-aqueous potassium-ion batteries: a review, Cur. Opin. Electrochem. 9 (2018) 41–48, https://doi.org/10.1016/j.coelec.2018.03.031.
[10] H. Kim, H. Ji, J. Wang, G. Ceder, Next-generation cathode materials for non-aqueous potassium-ion batteries, Trends Chem. 1 (7) (2019) 682–692, https://doi.org/10.1016/j.trechm.2019.04.007.
[11] T. Hosaka, K. Kubota, A.S. Hameed, S. Komaba, Research development on K-ion batteries, Chem. Rev. 120 (14) (2020) 6358–6466, https://doi.org/10.1021/acs.chemrev.9b00463.
[12] L. Fan, Y. Hu, A.M. Rao, J. Zhou, Z. Hou, C. Wang, B. Lu, Prospects of electrode materials and electrolytes for practical potassium-based batteries, Small Methods 5 (12) (2021) 2101131, https://doi.org/10.1002/smtd.202101131.
[13] S. Zhao, Z. Guo, K. Yan, X. Guo, S. Wan, F. He, B. Sun, G. Wang, The rise of Prussian blue analogs: challenges and opportunities for high-performance cathode materials in potassium-ion batteries, Small Struct. 2 (1) (2021) 2000054, https://doi.org/10.1002/sstr.202000054.
[14] T. Hosaka, T. Matsuyama, R. Tatara, Z.T. Gossage, S. Komaba, Impact of electrolyte decomposition products on the electrochemical performance of 4 V class K-ion batteries, Chem. Sci. 14 (33) (2023) 8860–8868, https://doi.org/10.1039/D3SC02111D.
[15] F. Allgayer, J. Maibach, F. Jeschull, Comparing the solid electrolyte interphases on graphite electrodes in K and Li half cells, ACS Appl Energy Mater 5 (1) (2022) 1136–1148, https://doi.org/10.1021/acsaem.1c03491.
[16] T. Hosaka, T. Matsuyama, R. Tatara, Z.T. Gossage, S. Komaba, Impact of electrolyte decomposition products on the electrochemical performance of 4 V class K-ion batteries, Chem. Sci. 14 (33) (2023) 8860–8868, https://doi.org/10.1039/D3SC02111D.
[17] A.J. Naylor, M. Carboni, M. Valvo, R. Younesi, Interfacial reaction mechanisms on graphite anodes for K-ion batteries, ACS Appl. Mater. Interfaces 11 (49) (2019) 45636–45645, https://doi.org/10.1021/acsami.9b15453.
[18] B. Larhrib, L. Madec, L. Monconduit, H. Martinez, A novel K-ion KVPO4F0.5O0.5/graphite full cell: correlation between XPS SEI studies and electrochemical testing results, J. Power Sources 588 (2023) 233743, https://doi.org/10.1016/j.jpowsour.2023.233743.
[19] L. Caracciolo, L. Madec, G. Gachot, H. Martinez, Impact of the salt anion on K metal reactivity in EC/DEC studied using GC and XPS analysis, ACS Appl. Mater. Interfaces 13 (48) (2021) 57505–57513, https://doi.org/10.1021/acsami.1c19537.
[20] A. Hofmann, F. Müller, S. Schöner, F. Jeschull, Revealing the formation of dialkyl dioxahexane dioate products from ethylene carbonate based electrolytes on lithium and potassium surfaces, Batter. Supercaps 6 (12) (2023) e202300325, https://doi.org/10.1002/batt.202300325.

[21] B. Larhrib, L. Madec, Toward highly reliable potassium-ion half and full coin cells, Batter. Supercaps 6 (5) (2023) e202300061, https://doi.org/10.1002/batt.202300061.
[22] S. Xing, A. Khudyshkina, U.-C. Rauska, A.J. Butzelaar, D. Voll, P. Theato, J. Tübke, F. Jeschull, Degradation of styrene-poly(ethylene oxide)-based block copolymer electrolytes at the Na and K negative electrode studied by microcalorimetry and impedance spectroscopy, J. Electrochem. Soc. 171 (4) (2024) 040516, https://doi.org/10.1149/1945-7111/ad3b72.
[23] H. Fei, Y. Liu, Y. An, X. Xu, J. Zhang, B. Xi, S. Xiong, J. Feng, Safe all-solid-state potassium batteries with three dimentional, flexible and binder-free metal sulfide array electrode, J. Power Sources 433 (2019) 226697, https://doi.org/10.1016/j.jpowsour.2019.226697.
[24] A.D. Khudyshkina, P.A. Morozova, A.J. Butzelaar, M. Hoffmann, M. Wilhelm, P. Theato, S.S. Fedotov, F. Jeschull, Poly(ethylene oxide)-based electrolytes for solid-state potassium metal batteries with a Prussian blue positive electrode, ACS Appl. Polym. Mater. 4 (4) (2022) 2734–2746, https://doi.org/10.1021/acsapm.2c00014.
[25] A.D. Khudyshkina, U.-C. Rauska, A.J. Butzelaar, M. Hoffmann, M. Wilhelm, P. Theato, F. Jeschull, Impact of nano-sized inorganic fillers on PEO-based electrolytes for potassium batteries, Batt. Supercaps 7 (1) (2024) e202300404, https://doi.org/10.1002/batt.202300404.
[26] W. Lyu, X. Yu, Y. Lv, A.M. Rao, J. Zhou, B. Lu, Building stable solid-state potassium metal batteries, Adv. Mater. 36 (24) (2024) 2305795, https://doi.org/10.1002/adma.202305795.
[27] W. Lyu, H. Fu, A.M. Rao, Z. Lu, X. Yu, Y. Lin, J. Zhou, B. Lu, Permeable void-free interface for all-solid-state alkali-ion polymer batteries, Sci. Adv. 10 (42) (2024) eadr9602, https://doi.org/10.1126/sciadv.adr9602.
[28] A.D. Khudyshkina, A.J. Butzelaar, Y. Guo, M. Hoffmann, T. Bergfeldt, M. Schaller, S. Indris, M. Wilhelm, P. Théato, F. Jeschull, From lithium to potassium: comparison of cations in poly(ethylene oxide)-based block copolymer electrolytes for solid-state alkali metal batteries, Electrochim. Acta 454 (2023) 142421, https://doi.org/10.1016/j.electacta.2023.142421.
[29] H. Fei, Y. Liu, Y. An, X. Xu, G. Zeng, Y. Tian, L. Ci, B. Xi, S. Xiong, J. Feng, Stable all-solid-state potassium battery operating at room temperature with a composite polymer electrolyte and a sustainable organic cathode, J. Power Sources 399 (2018) 294–298, https://doi.org/10.1016/j.jpowsour.2018.07.124.
[30] K. Xu, Nonaqueous liquid electrolytes for lithium-based rechargeable batteries, Chem. Rev. 104 (10) (2004) 4303, https://doi.org/10.1021/cr030203g.
[31] K. Xu, Electrolytes and interphases in Li-ion batteries and beyond, Chem. Rev. 114 (23) (2014) 11503–11618, https://doi.org/10.1021/cr500003w.
[32] M.P. Rosenwinkel, R. Andersson, J. Mindemark, M. Schönhoff, Coordination effects in polymer electrolytes: fast Li+ transport by weak ion binding, J. Phys. Chem. C 124 (43) (2020) 23588, https://doi.org/10.1021/acs.jpcc.0c08369.
[33] R. Andersson, G. Hernández, J. Mindemark, Quantifying the ion coordination strength in polymer electrolytes, Phys. Chem. Chem. Phys. 24 (26) (2022) 16343–16352, https://doi.org/10.1039/D2CP01904C.
[34] B. Sun, J. Mindemark, K. Edström, D. Brandell, Polycarbonate-based solid polymer electrolytes for Li-ion batteries, Solid State Ionics 262 (2014) 738–742, https://doi.org/10.1016/j.ssi.2013.08.014.
[35] J. Mindemark, B. Sun, E. Törmä, D. Brandell, High-performance solid polymer electrolytes for lithium batteries operational at ambient temperature, J. Power Sources 298 (2015) 166–170, https://doi.org/10.1016/j.jpowsour.2015.08.035.
[36] C. Sångeland, R. Younesi, J. Mindemark, D. Brandell, Towards room temperature operation of all-solid-state Na-ion batteries through polyester–polycarbonate-based polymer electrolytes, Energy Storage Mater 19 (2019) 31–38, https://doi.org/10.1016/j.ensm.2019.03.022.
[37] I. Johansson, R. Andersson, J. Erkers, D. Brandell, J. Mindemark, Polyester-polycarbonate polymer electrolytes beyond LiFePO4: influence of lithium salt and applied potential range, ChemElectroChem (2024) 11, https://doi.org/10.1002/celc.202400354.
[38] B. Park, R. Andersson, S.G. Pate, J. Liu, C.P. O'Brien, G. Hernández, J. Mindemark, J.L. Schaefer, Ion coordination and transport in magnesium polymer electrolytes based on polyester-co-polycarbonate, Energy Mater. Adv. (2021), https://doi.org/10.34133/2021/9895403.
[39] T.I. Kolesnikov, D. Voll, F. Jeschull, P. Theato, Synthesis of polyimide-PEO copolymers: toward thermally stable solid polymer electrolytes for lithium-metal batteries, Eur. Polym. J. 217 (2024) 113315, https://doi.org/10.1016/j.eurpolymj.2024.113315.
[40] J. Mindemark, E. Törmä, B. Sun, D. Brandell, Copolymers of trimethylene carbonate and ε-caprolactone as electrolytes for lithium-ion batteries, Polymer 63 (2015) 91–98, https://doi.org/10.1016/j.polymer.2015.02.052.
[41] J. Chen, K. Huang, S. Liu, Insoluble metal hexacyanoferrates as supercapacitor electrodes, Electrochem. Commun. 10 (12) (2008) 1851–1855, https://doi.org/10.1016/j.elecom.2008.07.046.
[42] X. Bie, K. Kubota, T. Hosaka, K. Chihara, S. Komaba, A novel K-ion battery: hexacyanoferrate(II)/graphite cell, J Mater Chem A 5 (9) (2017) 4325–4330, https://doi.org/10.1039/C7TA00220C.
[43] G. Hernández, I.L. Johansson, A. Mathew, C. Sångeland, D. Brandell, J. Mindemark, Going beyond sweep voltammetry: alternative approaches in search of the elusive electrochemical stability of polymer electrolytes, J. Electrochem. Soc. 168 (10) (2021) 100523, https://doi.org/10.1149/1945-7111/ac2d8b.
[44] G. Schwach, J. Coudane, R. Engel, M. Vert, More about the polymerization of lactides in the presence of stannous octoate, J. Polym. Sci. A Polym. Chem. 35 (16) (1997) 3431–3440, https://doi.org/10.1002/(SICI)1099-0518(19971130)35:16%253C3431::AID-POLA10%253E3.0.CO;2-G.
[45] A.A. Puchkov, N.G. Sedush, A.I. Buzin, T.N. Bozin, A.V. Bakirov, R.S. Borisov, S. N. Chvalun, Synthesis and characterization of well-defined star-shaped poly(L-Lactides), Polymer 264 (2023) 125573, https://doi.org/10.1016/j.polymer.2022.125573.
[46] A.P. Pêgo, A.A. Poot, D.W. Grijpma, J. Feijen, Physical properties of high molecular weight 1,3-trimethylene carbonate and D,L-lactide copolymers, J. Mater. Sci. Mater. Med. 14 (9) (2003) 767–773, https://doi.org/10.1023/a:1025084304766.
[47] L.Y. Tan, N. Chanthaset, H. Ajiro, Surface coating and characteristics of ester-free poly(trimethylene carbonate) bearing an aromatic urea moiety for biomaterials use, Mater. Adv. 3 (14) (2022) 5778–5785, https://doi.org/10.1039/D2MA00209D.
[48] J.S. Lyu, J.-S. Lee, J. Han, Development of a biodegradable polycaprolactone film incorporated with an antimicrobial agent via an extrusion process, Sci. Rep. 9 (1) (2019) 20236, https://doi.org/10.1038/s41598-019-56757-5.
[49] K.J. Zhu, R.W. Hendren, K. Jensen, C.G. Pitt, Synthesis, properties, and biodegradation of poly(1,3-trimethylene carbonate), Macromolecules 24 (8) (1991) 1736–1740, https://doi.org/10.1021/ma00008a008.
[50] S.I. Abdul Halim, C.H. Chan, H.-W. Kammer, About glass transition in polymer-salt mixtures, Polym. Test. 79 (2019) 105994, https://doi.org/10.1016/j.polymertesting.2019.105994.
[51] J. Mindemark, M.J. Lacey, T. Bowden, D. Brandell, Beyond PEO—alternative host materials for Li+-conducting solid polymer electrolytes, Prog. Polym. Sci. 81 (2018) 114–143, https://doi.org/10.1016/j.progpolymsci.2017.12.004.
[52] T. Eriksson, A. Mace, J. Mindemark, D. Brandell, The role of coordination strength in solid polymer electrolytes: compositional dependence of transference numbers in the poly(ε-caprolactone)–poly(Trimethylene carbonate) system, Phys. Chem. Chem. Phys. 23 (45) (2021) 25550–25557, https://doi.org/10.1039/D1CP03929F.
[53] R. Andersson, C. Mönich, G. Hernández, M. Schönhoff, J. Mindemark, Transference numbers and ion coordination strength for Mg2+, Na+, and K+ in solid polymer electrolytes, J. Phys. Chem. C 128 (39) (2024) 16393–16399, https://doi.org/10.1021/acs.jpcc.4c04632.
[54] J.U. Izunobi, C.L. Higginbotham, Polymer molecular weight analysis by 1H NMR spectroscopy, J. Chem. Educ. 88 (8) (2011) 1098–1104, https://doi.org/10.1021/ed100461v.
[55] L. Wildersinn, D. Stottmeister, F. Jeschull, A. Groß, A. Hofmann, Decomposition of binary mixtures of DMC/EC, EMC/EC, and DEC/EC on potassium surfaces; GC, XPS, and calculation, ACS Appl. Mater. Interfaces 17 (6) (2025) 10055–10072, https://doi.org/10.1021/acsami.4c17461.
[56] A.P. Pêgo, A.A. Poot, D.W. Grijpma, J. Feijen, Biodegradable elastomeric scaffolds for soft tissue engineering, J. Control. Release 87 (1) (2003) 69–79, https://doi.org/10.1016/S0168-3659(02)00351-6.
[57] J. Mindemark, A. Sobkowiak, G. Oltean, D. Brandell, T. Gustafsson, Mechanical stabilization of solid polymer electrolytes through gamma irradiation, Electrochim. Acta 230 (2017) 189–195, https://doi.org/10.1016/j.electacta.2017.02.008.